Sequential geoacoustic inversion at the continental shelfbreak

Caglar Yardim,[a] Peter Gerstoft, and William S. Hodgkiss
Marine Physical Laboratory, Scripps Institution of Oceanography, La Jolla, California 92093-0238

(Received 2 May 2011; revised 17 August 2011; accepted 21 August 2011)

Environmental parameters can have large spatial and temporal variability in shelfbreak regions. The capability of sequential Bayesian filters in tracking this variation is investigated. Particle filtering (PF) is used to extract the environmental parameters and their uncertainties. The method tracks the environment with fewer particles relative to conventional geoacoustic inversion methods using successive independent inversions. As an example, data from the Shallow Water 2006 Experiment are processed. The PF approach first is used to track the source and the environment with little spatial variation just northwest of the shelfbreak. Then the strongly range-dependent shelfbreak region is analyzed and the PF results are compared to previous geoacoustic inversion studies from the region. © *2012 Acoustical Society of America*. [DOI: 10.1121/1.3666012]

PACS number(s): 43.30.Pc, 43.60.Pt, 43.60.Wy, 43.60.Jn [AIT] Pages: 1722–1732

I. INTRODUCTION

The ocean shelfbreak region is characterized by rapid change in bathymetry, large variations in geoacoustic parameters, and the ocean sound speed can evolve rapidly both temporally and spatially due to the interplay between deep and shallow water. Sequential Bayesian filters offer a suitable framework for extracting geoacoustic parameters in such a dynamic environment. They tie together information on parameter evolutions, a forward model relating acoustic field measurements to the unknown quantities, and a statistical description of the random perturbations in the field measurements. A review of sequential filtering in ocean acoustics is given in Ref. 1 with several underwater acoustic applications such as target localization and tracking,[2–4] sequential geoacoustic inversion,[5–8] frequency tracking,[9] and spatial arrival time tracking.[10]

Recently, there has been interest in addressing the capabilities of geoacoustic inversion at the continental shelfbreak regions. Shallow Water 2006[11] (SW06) was a series of experiments conducted in the summer of 2006 in the vicinity of the New Jersey continental shelfbreak.[12] In addition to the spatial and temporal variabilities of the water column, this shelfbreak region is characterized by the presence of internal waves. Sediment properties at the site such as the sound speed, dispersion, and attenuation were measured *in situ*.[13,14] The seismic surveys showed a significant R-reflector at the SW06 site[15,16] that corresponds to a subsurface layer with abrupt sediment sound speed change. This R-reflector is around 20–25 m below the seafloor[17,18] and its spatial variability around the SW06 site has been observed.[19,20]

Geoacoustic inversion methods[21–25] have been used to invert for the seabed properties in this challenging environment. An iterative scheme is used with a dispersion-based short time Fourier transform.[21] Spatial variability is tackled by incorporating the locations of the R-reflector and other layering information into the perturbative inversion as *a priori* information.[22] Matched-field Bayesian geoacoustic inversion algorithms[24,25] used with SW06 data incorporate empirical orthogonal functions (EOF) to represent the high temporal variability of the sound speed profile (SSP) in the water column.

Sequential Monte Carlo techniques known as particle filters (PF) perform well in matched-field shallow water geoacoustic inversion applications.[6] Two environmental parameter models for the PF are considered here depending on the complexity of the environment. The first is appropriate for slowly varying bathymetry and geoacoustic parameters. It assumes gradual range dependence and uses the adiabatic normal mode model SNAPRD.[26] The gradual range dependence is obtained by calculating the mode functions at the source and receiver locations and linearly interpolating the wavenumbers along the track.[7]

The second geoacoustic parameter model deals with a complex, fast-changing bathymetry. This uses a wide-angle parabolic equation with Padé coefficients as in the range-dependent acoustic model.[27] The state vector now incorporates the bathymetry from all ranges to compute the field. However, this improved ability to track complicated seabed properties means that the increasing state dimension ultimately will limit the length of the track. To keep the state size manageable, the full track is split into smaller tracks and a PF is run for each sector.

The paper is organized as follows. Section II introduces the PF and the two environmental parameter models that are used in this paper. An improved likelihood for the PF also is introduced, along with the PF equations and the sequential importance resampling (SIR) algorithm. Section III shows the application of PF on data obtained from SW06, both in the weakly and strongly range-dependent regions, followed by discussion and conclusions.

II. GEOACOUSTIC PARTICLE FILTERS

Particle filters enable tracking of evolving geoacoustic parameters via sequential observations. These techniques provide a formulation where the environmental parameters such as the ocean SSP and sediment properties are

[a]Author to whom correspondence should be addressed. Electronic mail: cyardim@ucsd.edu

characterized as dynamic, non-stationary processes that are continuously estimated as new data become available. This is done by employing predictions from previous estimates and updates stemming from physical and statistical models that relate acoustic measurements to the unknown parameters.

The objective of a PF is to track the evolution of the multidimensional posterior probability density function (PDF) $p(\mathbf{x}_t|\mathbf{y}_0,\ldots,\mathbf{y}_t)$; the probability of the unknown geoacoustic parameters $\mathbf{x}_t$ given the measurements $\mathbf{y}$ up to and including time t. The PF achieves this by creating a set of $i=1,\ldots,n_p$ particles $\mathbf{x}_t^i$, each with weight w_t^i, where the weighted sum of these particles approximate the posterior PDF,

$$\chi_t : \{\mathbf{x}_t^i, w_t^i\}_{i=1}^{n_p},$$
$$p(\mathbf{x}_t|\mathbf{y}_0,\ldots,\mathbf{y}_t) \cong \sum_{i=1}^{n_p} w_t^i \delta(\mathbf{x}_t - \mathbf{x}_t^i). \quad (1)$$

Geoacoustic inversion uses an acoustic measurement equation that relates the environment and the source location to the acoustic field. In addition to the measurement equation, tracking via PF involves a state equation that models the evolution of the environment and movement of the source. Usually, but not necessarily, the field is measured across a receiver array. The equations are given as[7]

$$\mathbf{x}_t = \mathbf{f}_{t-1}(\mathbf{x}_{t-1}) + \mathbf{B}_t\mathbf{v}_t, \quad (2)$$

$$\mathbf{y}_t = \mathbf{h}_t(\mathbf{x}_t) + \mathbf{w}_t = a_t\mathbf{d}(\mathbf{x}_t) + \mathbf{w}_t, \quad (3)$$

where $\mathbf{f}_{t-1}(\cdot)$ is a known function of the state vector $\mathbf{x}_{t-1}$ and $\mathbf{h}_t(\cdot)$ is the known nonlinear function that relates the environmental and source parameters $\mathbf{x}_t$ to the acoustic measurement vector $\mathbf{y}_t$. Hence, $\mathbf{h}_t(\cdot)$ includes both the unknown source amplitude term a_t and the known forward model $\mathbf{d}(\mathbf{x}_t)$. $\mathbf{v}_t$, $\mathbf{w}_t$, and $\mathbf{B}_t$ are the process/state noise vector, the measurement noise vector, and the scaling matrix. $\mathbf{Q}_t$ and $\mathbf{R}_t$ are the covariance matrices at t for the corresponding noise terms. The scaling matrix $\mathbf{B}_t$ is not needed for the environmental parameters and is taken as the identity matrix $\mathbf{I}$ but it is needed in the source model. All the functions, parameters, and the noise terms are time dependent, which enables the PF to work in dynamic, non-stationary environments.

The state equation is formed from two blocks; source and environmental parameter blocks. In the source block, three source parameters (i.e., source depth, range, and radial speed) are grouped as $\mathbf{s}_t = [z_s\, r_s\, v_s]_t'$. Using a constant velocity track model for the source, the source block in the state equation is given by

$$\mathbf{s}_t = \mathbf{F}^{\mathbf{s}}\mathbf{s}_{t-1} + \mathbf{B}^{\mathbf{s}}\mathbf{v}_t^{\mathbf{s}}, \quad (4)$$

$$\begin{bmatrix} z_s \\ r_s \\ v_s \end{bmatrix}_t = \begin{bmatrix} 1 & 0 & 0 \\ 0 & 1 & \Delta t \\ 0 & 0 & 1 \end{bmatrix} \begin{bmatrix} z_s \\ r_s \\ v_s \end{bmatrix}_{t-1} + \begin{bmatrix} 1 & 0 \\ 0 & \frac{\Delta t^2}{2} \\ 0 & \Delta t \end{bmatrix} \begin{bmatrix} v_{z_s} \\ v_{a_s} \end{bmatrix}_t, \quad (5)$$

where Δt is the time between successive measurements, v_{z_s} and v_{a_s} are random variables representing the variation in source depth and acceleration, respectively.[28] The PF allows for any type of PDF to be used for these two variables. However, small fluctuations around the mean speed for a source moving with a constant velocity can be characterized adequately by introducing an acceleration error term with a zero-mean Gaussian PDF. Note that the posterior PDFs for the geoacoustic and source parameter estimates are not Gaussian even though the noise terms v_{z_s} and v_{a_s} are assumed Gaussian.

The initial density for the environment and source location $p(\mathbf{x}_0)$ can take into account any prior knowledge that is available or instead $p(\mathbf{x}_0/\mathbf{y}_0)$ can be used, by running a geoacoustic inversion employing a Monte Carlo sampler[29] at $t=0$. As the PF can operate on non-Gaussian densities, any PDF can be used. The effect of the prior will diminish rapidly with time as more and more data are used in the track.

A. State vector for weakly range-dependent geoacoustic parameters

Gradual range dependence allows for a simple formulation where the environmental parameters (water depth, SSP, and sediment parameters) at step t are grouped into $\mathbf{m}_t$ to form the environmental block.[6] The environmental component of the state vector only consists of the environment at the location of the moving source. This model assumes that the rate of change of the environment is slow for each time step. Hence, the environmental block has both $\mathbf{F}^{\mathbf{m}}$ and $\mathbf{B}^{\mathbf{m}}$ taken as identity matrices in Eq. (2), giving $\mathbf{m}_t = \mathbf{F}^{\mathbf{m}}\mathbf{m}_{t-1} + \mathbf{B}^{\mathbf{m}}\mathbf{v}_t^{\mathbf{m}} = \mathbf{m}_{t-1} + \mathbf{v}_t^{\mathbf{m}}$. Here, $\mathbf{v}^{\mathbf{m}}$ is the state noise matrix for the environmental parameters that takes into account the error in the evolution model. This noise term enables the filter to continue tracking the environment even when the evolution in environmental parameters differs from the model evolution defined by the state equation, such as when there is a rapid change in the environment in one step.

The full state vector merges both the source and the environmental parameters. Hence, the state equation is obtained by merging the two blocks. Defining the state vector as $\mathbf{x}_t' = [\mathbf{s}_t'\ \mathbf{m}_t']$, the state equation, Eq. (2), for gradual range dependence is obtained as

$$\begin{bmatrix} \mathbf{s} \\ \overline{\mathbf{m}} \end{bmatrix}_t = \begin{bmatrix} \mathbf{F}^{\mathbf{s}} & 0 \\ 0 & \mathbf{I} \end{bmatrix} \begin{bmatrix} \mathbf{s} \\ \overline{\mathbf{m}} \end{bmatrix}_{t-1} + \begin{bmatrix} \mathbf{B}^{\mathbf{s}} & 0 \\ 0 & \mathbf{I} \end{bmatrix} \begin{bmatrix} \mathbf{v}^{\mathbf{s}} \\ \overline{\mathbf{v}_{\mathbf{m}}} \end{bmatrix}_t. \quad (6)$$

Note that both $\mathbf{F}^{\mathbf{s}}$ and $\mathbf{B}^{\mathbf{s}}$ are time independent. Similarly, $\mathbf{v}^{\mathbf{s}}$ and $\mathbf{v}^{\mathbf{m}}$ are stationary random variables with constant $\mathbf{Q}$. In Eq. (3), $\mathbf{d}(\cdot)$ is implemented using the adiabatic normal mode model SNAPRD for the data analyses discussed in Sec. III.

B. State vector for strongly range-dependent geoacoustic parameters

A complicated bathymetry requires a larger number of interpolation points along the propagation path. Assume a source moving away from a receiver array over a highly range-dependent region and $\mathbf{m}_t(r_t)$ is the environment at range r_t under the moving source at time t. Environments at all previous ranges are included in the state vector $\mathbf{x}_t$ in addition to the environment at the current location and the source

parameters. The acoustic signal $\mathbf{y}_t$ measured by the receiver array at r_t depends on $\mathbf{m}_t(r_\tau)$ for all $\tau \le t$. For a track that runs T steps, the state vector and the measurement equations assume the form

$$\mathbf{x}_t = [\mathbf{s}'\mathbf{m}'(r_0)\cdots\mathbf{m}'(r_t)\cdots\mathbf{m}'(r_T)]'_t, \tag{7}$$

$$\mathbf{y}_t = a_t\mathbf{d}\left([\mathbf{m}'(r_0)\cdots\mathbf{m}'(r_t)]'_t\right), \tag{8}$$

where r_0 represents the source range at the first time step of the filter and the forward model $\mathbf{d}(\cdot)$ is selected as a wide-angle parabolic equation code. Only the parameters in $\mathbf{x}_t$ representing the region up to the source range are used in the measurement equation.

The source modeling in the state equation is as in Eq. (5). The geoacoustic portion of the state equation is formulated using

$$\mathbf{m}_t(r_k) = \begin{cases} \mathbf{m}_{t-1}(r_k) + \mathbf{v}_{\text{temp}} & k < t \\ \mathbf{m}_{t-1}(r_{k-1}) + \mathbf{v}_{\text{spat}} & k = t, \end{cases} \tag{9}$$

where $\mathbf{v}_{\text{temp}}$ and $\mathbf{v}_{\text{spat}}$ are temporal and spatial state noise terms, respectively. This definition enables the PF to take into account both the spatial and temporal coherence in the evolution of parameters in the state equation. The predict and update stages of a single particle at t are shown in Fig. 1. All the environmental parameters up to and including t in the particle are predicted via Eq. (9). Then the acoustic field across the array for the environment represented by this particle is computed via the forward model $\mathbf{d}(\cdot)$. Afterward, the likelihood of this particle is computed using the acoustic data. Once the likelihoods of all particles are computed, the posterior PDF of the environmental parameters is computed via importance sampling using the weight of each particle. Finally, a new set of particles is created at the resampling stage, where the number of particles in a region of the state space will be proportional to the value of the posterior PDF at that location. This completes the update stage of the PF and the filter moves to the next step. Note that the unused terms relating to ranges greater than r_t in the state vector [Eq. (7)] are excluded both from the state and measurement equations, Eqs. (8) and (9).

Hence, the full state equation takes the form

$$\begin{bmatrix} \mathbf{s} \\ \hline \mathbf{m}(r_0) \\ \vdots \\ \mathbf{m}(r_{t-1}) \\ \hline \mathbf{m}(r_t) \end{bmatrix}_t = \begin{bmatrix} \mathbf{F}^{\mathbf{s}} & 0 \\ 0 & \mathbf{I} \\ 0 & 0\cdots 0\mathbf{I} \end{bmatrix} \begin{bmatrix} \mathbf{s} \\ \hline \mathbf{m}(r_0) \\ \vdots \\ \mathbf{m}(r_{t-1}) \end{bmatrix}_{t-1} + \mathrm{B}\mathrm{v}_t, \tag{10}$$

where the state parameters are separated as the source terms, temporally updated environmental terms, and spatially updated environmental terms. If the spatial variation is too large, the last line in Eq. (10) can be modeled as $[\mathbf{0}\cdots\mathbf{0}-\mathbf{I}\ \mathbf{2I}]$ as $\mathbf{m}_t(r_t) = \mathbf{m}_{t-1}(r_{t-1}) + \Delta\mathbf{m}_{t-1}$ with the spatial rate of change in $\mathbf{m}$ estimated by $\Delta\mathbf{m}_{t-1} = \mathbf{m}_{t-1}(r_{t-1}) - \mathbf{m}_{t-1}(r_{t-2})$. This takes into account the rate of change of the parameter assuming the ship speed is constant. Another way would be to include the rates of change $(\partial\mathbf{m}/\partial r)$ as separate parameters to be tracked.

As an example, assume water depth ($\mathbf{m} = wd$) is tracked over the shelfbreak. At $t = 0$ the acoustic data $\mathbf{y}_0$ is inverted, giving a source range of r_0 with a water depth of $wd_0(r_0)$. At $t = 1$, the source moves to r_1. Acoustic data $\mathbf{y}_1$ provide the first time information about wd at r_1 as well as extra information about the already-estimated parameter wd at r_0. Therefore the PF with a state equation as given in Eq. (9) can correct the previous estimate $\widehat{wd}_{t=0}(r_0)$ at $t = 1$ giving $\widehat{wd}_1(r_0)$, and estimate $wd_1(r_1)$ for the first time.

Following the first line in Eq. (9), $wd_1(r_0)$ will be predicted to be its own previously estimated value $wd_0(r_0)$ with the addition of a temporal noise term. This noise term allows the PF to correct the previous estimate at the same location if it changed between the two measurements. It also allows for a correction in the parameter at that range in case the ship motion is not entirely in a radial direction. On the other hand, there is no previous information on wd at r_1 so the value at the closest known value $wd_0(r_0)$ will be assigned to it with an additive spatial noise term that will allow the PF to take into account the difference between the water depth in the two locations.

Therefore, as the ship moves, there will be $t+1$ data sets $\mathbf{Y}_t = \{\mathbf{y}_0, \mathbf{y}_1, \ldots, \mathbf{y}_t\}$ that are used to extract $wd(r_0)$, t for $wd(r_1)$, etc., and only the data $\mathbf{y}_t$ for $wd(r_t)$. As long as the ship moves radially, the location of $wd(r_0)$ does not change with time. This means the output of the PF at r_0 is effectively $p(wd(r_0)|\mathbf{Y}_t)$, a behavior similar to a particle smoother even though we are running a PF.[1]

An efficient implementation of a strongly range-dependent state model is splitting the total track length T into smaller tracks 0: T_1: $T_2\cdots T$. The PF is then run on each track successively, where the posterior of the first PF at T_1 is used as the prior for the next PF. As a short section of the total track is used in each PF run, the dimension of the state, which contains the environmental parameters at each range, remains small. The trade-off is that only the data in the smaller track will be used to estimate the local parameters.

Finally, a mixed state formulation can be used, where some parameters are modeled as explained earlier and others as in Sec. II A. Hence, the mixed model will have weakly

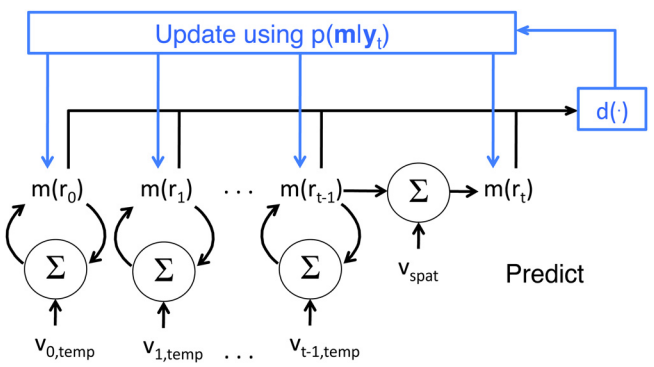

FIG. 1. (Color online) Predict and update for a particle for strongly range-dependent environment at time t.

range-dependent $\mathbf{m}$ modeled as given in Eq. (6), whereas the strongly range-dependent parameters will follow Eq. (10). For the SW06 site, the bathymetry changes between 60 and 500 m. However, the R-reflector is much more stable, at 20–25 m below the seafloor, following closely the bathymetry line. Similarly, the sound speed, attenuation, and densities of sediment layers are relatively stable.[19] Thus, a mixed state model appropriate for SW06 environment treats the water depth as strongly range dependent and sediment and SSP parameters as weakly range dependent.

C. Likelihood formulation

Previously, a PF likelihood formulation[7] was developed based on the classical geoacoustic inversion likelihood obtained from the Bartlett power objective function.[30] That likelihood function used all the state parameters except ship speed. Here, an improved likelihood function is adopted as the ship speed parameter also is incorporated.

The classical Bartlett power objective function is obtained from the assumption of additive complex Gaussian noise $\mathbf{w}_t(f_j)$ for each frequency f_j and step t, which is written as $\mathbf{w}_t(f_j) = \mathbf{y}_t(f_j) - a_t(f_j)\mathbf{d}(\mathbf{x}_t, f_j)$ following Eq. (3), with a corresponding Bartlett processor based, multifrequency likelihood function:

$$\mathcal{L}(\mathbf{x}_t) = \prod_{j=1}^{n_\mathrm{f}} \frac{1}{(\pi\nu_j)^{n_\mathrm{h}}} \exp\left[-\frac{\left\|\mathbf{y}_t(f_j) - a_t(f_j)\mathbf{d}(\mathbf{x}_t, f_j)\right\|^2}{\nu_j}\right], \quad (11)$$

where n_h and n_f are the numbers of hydrophones and the frequencies used in tracking, and ν_j is the noise variance at frequency f_j. The unknown source complex amplitude is estimated by a maximum likelihood estimator. An analytic solution is obtained by solving $\partial\mathcal{L}/\partial a_t = 0$:

$$\hat{a}_t(f_j) = \frac{\mathbf{d}(\mathbf{x}_t, f_j)^H \mathbf{y}_t(f_j)}{\left\|\mathbf{d}(\mathbf{x}_t, f_j)\right\|^2}. \quad (12)$$

Inserting the source estimate back into Eq. (11), the cross spectral density matrix (CSDM) is defined as the average CSDM obtained from n data snapshots collected between $t-1$ and t:

$$\mathbf{C}_t(f_j) \approx \frac{1}{n}\sum_{i=1}^{n} \mathbf{y}_t(i, f_j)\mathbf{y}_t(i, f_j)^\mathrm{H}. \quad (13)$$

Then the likelihood is written as[30,31]

$$\phi_j(\mathbf{x}_t) = \mathrm{tr}\mathbf{C}_t(f_j) - \frac{\mathbf{d}(\mathbf{x}_t, f_j)^\mathrm{H}\mathbf{C}_t(f_j)\mathbf{d}(\mathbf{x}_t, f_j)}{\mathbf{d}(\mathbf{x}_t, f_j)^\mathrm{H}\mathbf{d}(\mathbf{x}_t, f_j)}, \quad (14)$$

$$\mathcal{L}(\mathbf{x}_t) = \prod_{j=1}^{n_\mathrm{f}} \frac{1}{(\pi\nu_j)^{n_\mathrm{h}}} \exp\left[-\frac{\phi_j(\mathbf{x}_t)}{\nu_j}\right], \quad (15)$$

where tr is the trace operation, ν is the noise variance, and ϕ_j is the Bartlett objective function. A frequency-coherent Bartlett objective function can also be used as the PF will help eliminate range aliasing accompanied by undersampling in the frequency domain.[32]

The predicted ship speed at $t-1$ can be used to obtain an evolving objective function corrected for the ship motion, instead of an ensemble average. Unlike a geoacoustic inversion problem, the PF tracks readily the source speed so the PF enables us to predict where the source is going to be at each snapshot between $t-1$ and t. Assuming n snapshots, the range, geoacoustic parameters, and the outer product of the data vector at the ith snapshot are given by

$$r_t(i) = r_{t-1} + \frac{i}{n}\Delta t v_{s_{t-1}}, \quad (16)$$

$$\mathbf{x}_t(i) = \mathbf{x}_{t-1} + \frac{i}{n}(\mathbf{x}_t - \mathbf{x}_{t-1}), \quad (17)$$

$$\mathbf{C}_t(i, f_j) = \mathbf{y}_t(i, f_j)\mathbf{y}_t(i, f_j)^\mathrm{H}, \quad (18)$$

with the corresponding Bartlett and likelihood functions:

$$\phi_{ij}(\mathbf{x}_t) = \mathrm{tr}\mathbf{C}_t(i, f_j) - \frac{\mathbf{d}(\mathbf{x}_t(i), f_j)^\mathrm{H}\mathbf{C}_t(i, f_j)\mathbf{d}(\mathbf{x}_t(i), f_j)}{\mathbf{d}(\mathbf{x}_t(i), f_j)^\mathrm{H}\mathbf{d}(\mathbf{x}_t(i), f_j)}, \quad (19)$$

$$\mathcal{L}(\mathbf{x}_t) = \prod_{i=1}^{n}\prod_{j=1}^{n_\mathrm{f}} \frac{1}{(\pi\nu_{ij})^{n_\mathrm{h}}} \exp\left[-\frac{\phi_{ij}(\mathbf{x}_t)}{\nu_{ij}}\right]. \quad (20)$$

Treating the unknown noise variance v as a nuisance parameter, we again can use a maximum likelihood estimator similar to the unknown source estimation performed earlier. Solving $\partial\mathcal{L}/\partial\nu = 0$ results in[31]

$$\hat{\nu}_{ij} = \frac{\phi_{ij}(\mathbf{x}_t)}{n_\mathrm{h}}. \quad (21)$$

Inserting Eq. (21) into Eq. (20), the likelihood used in this paper is obtained as

$$\mathcal{L}(\mathbf{x}_t) = \prod_{i=1}^{n}\prod_{j=1}^{n_\mathrm{f}} \left(\frac{n_\mathrm{h}}{\mathrm{e}\pi\phi_{ij}(\mathbf{x}_t)}\right)^{n_\mathrm{h}}. \quad (22)$$

D. Filter implementation

A SIR (Refs. 1 and 33) type PF is used in this work. The PF is a sequential Monte Carlo method that is used to track desired parameters and their underlying PDFs in a dynamic non-linear, non-Gaussian system as they evolve both in space and time.[28,34]

The SIR algorithm uses a set of n_p particles $\{x_t^l\}_{l=1}^{n_\mathrm{p}}$ to represent the PDF at each step t. The filter has predict and update sections which the SIR algorithm uses first for predicting the next set of values of the environmental and source parameters given their previous history and then including the latest measurement to correct/update the predicted value and their PDFs. The initial set of particles

$\{x_0^l\}_{l=1}^{n_p}$ are sampled from the prior $p(\mathbf{x}_0)$. A single iteration at step t of the SIR is summarized as follows.

(1) *Predict:* For a given set of particles from the previous step $\{x_{t-1}^l\}_{l=1}^{n_p}$, create a new set $\{x_{t|t-1}^l\}_{l=1}^{n_p}$ by using Eq. (2). Hence, predict where each particle should be at the current step given its previous location.

(2) *Update:* Update the predictions in the previous step using the acoustic data that just came in at the current step t. Calculate the normalized weight W_t^l of each particle $x_{t|t-1}^l$ from its likelihood function:

$$\mathcal{L}\left(\mathbf{x}_{t|t-1}^i\right) = \prod_{i=1}^{n}\prod_{j=1}^{n_f}\left(\frac{n_h}{e\pi\phi_{ij}\left(\mathbf{x}_{t|t-1}^i\right)}\right)^{n_h}, \tag{23}$$

$$w_t^l = \frac{\mathcal{L}\left(\mathbf{x}_{t|t-1}^l\right)}{\sum_{l'=1}^{n_p}\mathcal{L}\left(\mathbf{x}_{t|t-1}^{l'}\right)}. \tag{24}$$

The posterior PDF $p(\mathbf{x}_t/\mathbf{x}_{t-1}, \mathbf{y}_t)$ now can be approximated using importance sampling:

$$p\left(\mathbf{x}_t\middle|\mathbf{x}_{t-1}, \mathbf{y}_t\right) = \sum_{l'=1}^{n_p} w_t^{l'}\delta\left(\mathbf{x}_t - \mathbf{x}_t^{l'}\right). \tag{25}$$

(3) *Resample:* Create a new set of particles denoted by $\{x_{t|t}^l\}_{l=1}^{n_p}$ by resampling $\{x_{t|t-1}^l\}_{l=1}^{n_p}$, effectively integrating both the predictions from previous values and the information coming from the new measurement. Resampling generates particles with identical weights from the parent set according to the weights of the parent particles, with high likelihood particles generating more particles than the low likelihood ones.[28]

III. SHALLOW WATER 2006

The shelfbreak region in SW06 is shown in Fig. 2. The isobath lines lie diagonally southwest–northeast with the northwest of the shelf characterized by a flat region at 80 m water depth. Track I is a 30 min long radial track starting northeast of vertical line array VLA1 moving toward the array, whereas Track II is perpendicular to the isobaths, crossing over the shelfbreak. This section is composed of two examples:

(1) Tracking in a relatively range-independent area (Track I) northwest of the shelfbreak. Data were collected on August 28, 2006 (JD240), 00:50–01:20 UTC.
(2) Tracking across the shelfbreak (Track II) with strong range dependence. Data were collected on August 28, 2006 (JD240), 02:12–09:00 UTC.

Both data sets were recorded by the 16-element, 56.25 m aperture VLA1 moored at 39°1.477′N, 73°2.256′W at a water depth of 79 m. The bottom hydrophone is 8.2 m above the seafloor. Due to mechanical strum contamination in the upper array elements, only the lower ten array elements are used in the analysis.

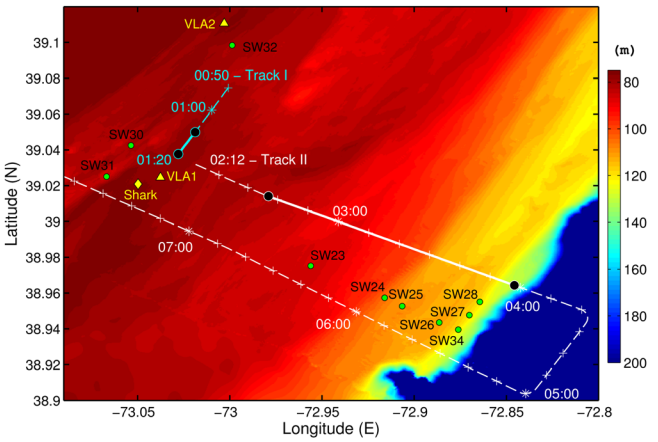

FIG. 2. (Color online) SW06 bathymetry and ship tracks. SW23–SW34 represent environmental moorings. Shark, VLA1, and VLA2 represent acoustic arrays. Entire ship tracks are given in dashed lines. Start/end of the sections used in tracking (solid) are marked with closed circles.

A. Track I data

As the environmental variation is small, the formulation in Sec. II A is adopted as given in Eq. (6). The source location, bathymetry, array parameters, and the seabed properties are assumed unknown. The R/V Knorr approached the array with a speed of 5 kn, simultaneously towing a source at 25–30 m depth and emitting a multitone comb at frequencies 303, 403, 503, 703, and 953 Hz. The last 10 min section of Track I ranging from 3.5 to 1.5 km is used. The data from this track also were inverted in Refs. 24 and 25.

The received time series was split into snapshots with 50% overlap and converted to the frequency domain using a 2^{18}-point fast Fourier transform. The data CSDMs were computed as the outer products of seven snapshots representing a time epoch of 20 s spread across 50 m in range, hence 30 time steps for a track length of 10 min in the PF.

The environment model given in Fig. 3 is used for each range. For this case, the sediment sound speed is taken as a constant with $\Delta c_{sed} = 0$. An EOF analysis of the SSP was carried out using 16 conductivity, temperature, depth sensor (CTD) measurements along the 80 m isobath track from JD239 19:17 to JD243 20:16 UTC giving a mean profile together with the first three EOFs (accounting for 90% of the variance in ocean SSP).[25] The SSP is tracked by tracking the EOF coefficients.

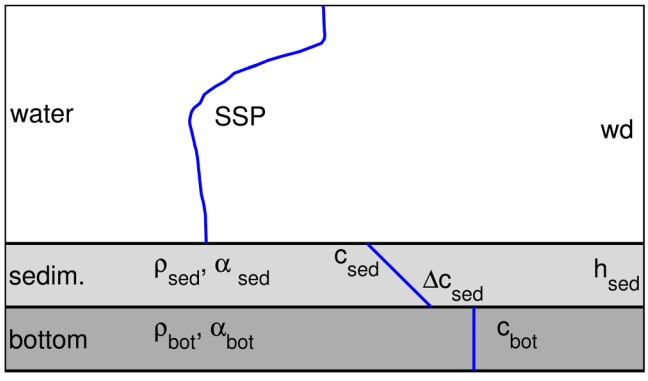

FIG. 3. (Color online) Geoacoustic model used in the inversions.

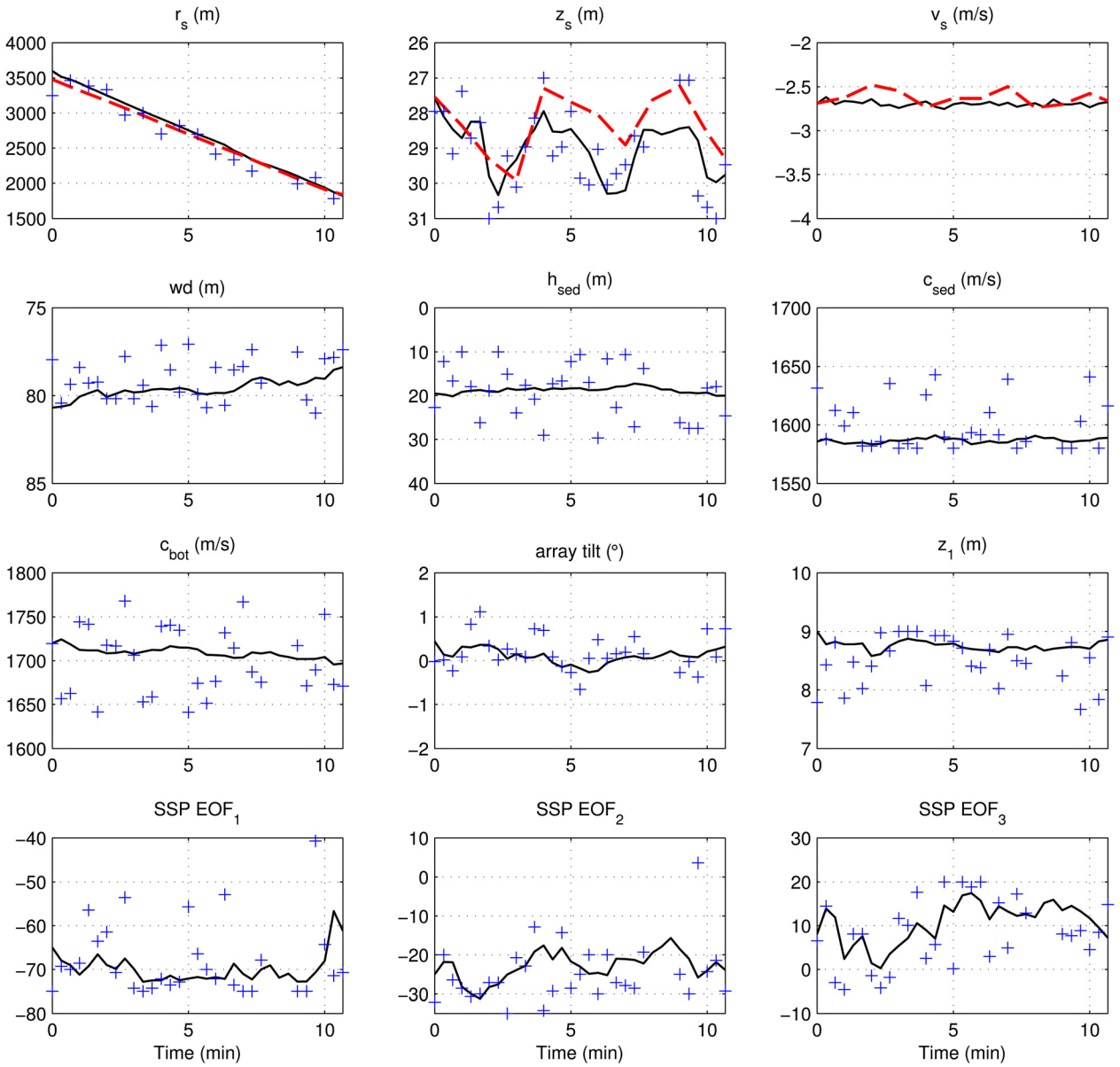

FIG. 4. (Color online) Track I results for the source (top) and geoacoustic parameters using GA (+) and PF (solid), together with the true trajectories (dashed).

Bartlett processor based likelihood functions are computed from Eqs. (15) and (22) to be used in genetic algorithms (GA) and the PF, respectively. First, data at each time step are inverted independently by a global optimizer (using a 30 000-point GA). Tracking can be achieved using a small number of particles.[7] Obtaining a smooth posterior PDF requires more particles, but still less than for GA. Hence, the source and receiver VLA parameters, the SSP, and the geoacoustic parameters are tracked using a 5000-point SIR PF. The root-mean-square (rms) error decreases with increased number of particles, albeit with decreasing benefit (see Fig. 4 in Ref. 6) and the n_p needed to obtain accurate PDFs is a function of the number of parameters, the specifics of the state space formulation, and the importance sampling density.

True source depth, range, and speed values are obtained using global positioning system (GPS) and depth sensor data. z_1 is the distance between the deepest element in the array and the seafloor. The results are given in Fig. 4. For the GA runs, the source range is assumed to be known within a 500 m limit around its true value at any t. The PF does not use such prior information and has a range limit of 0–5000 m for the moving source. The rms errors between the ground truth values and the inversion results for r_s, v_s, and z_s for PF (GA) are 32.3 (68.4) m, 0.09 (0.8) m/s, 1.06 (1.31) m, respectively. Note that the source depth fluctuates between 27 and 30 m depth. Even though a constant-depth source evolution model is used, the PF still tracks the source depth fluctuations due to the state noise that compensates for the evolution model errors. As successive GA inversions do not take advantage of the previous steps, the GA results have a larger variation than the PF results, particularly in c_{bot}, h_{sed}, and the SSP EOFs.

The evolving marginal posterior PDFs for the source, geoacoustic parameters, and SSP EOFs are all given in Fig. 5. The water depth slowly decreases from 81 to 78 m. The sediment sound speed stays between 1580 and 1605 m/s, sediment thickness 17–22 m, and the bottom sound speed

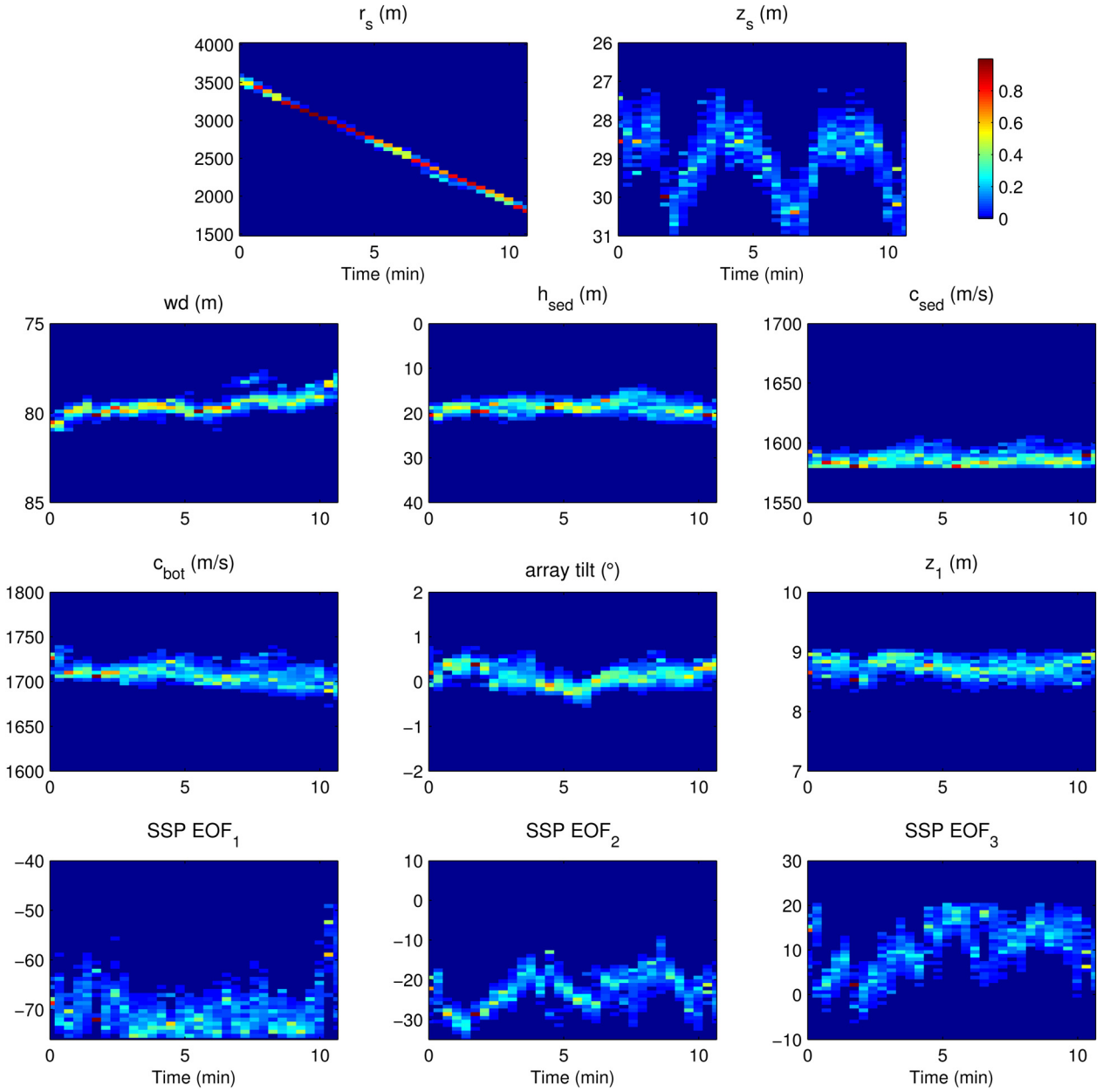

FIG. 5. (Color online) Track I results as evolving marginal PDFs for source location, sediment thickness, and SSP EOF parameters given as a normalized histograms of particles.

1690–1750 m/s, respectively, along the track. Even though detailed range-dependent ground truth measurements do not exist, the results compare favorably with previous studies that inverted data from the same area with an average c_{sed} of 1599 (Ref. 24) (1604—Ref. 25) m/s, h_{sed} of 21.1 (24) m, and c_{bot} of 1740 (1739) m/s. Sediment thickness is consistent with other studies where the R-reflector is found to be around 20 m below the seafloor.[17–20] Previous studies[14,22,23] also reported similar sediment sound speed results.

B. Track II data

In Track II, the source starts close to VLA1 and moves away from the receiver at a speed of 5 kn across the shelfbreak. The source is towed at a depth of 28–32 m, emitting four continuous wave (CW) tonals (53, 103, 203, and 253 Hz). The PF track covers ranges from 5 to 18 km (80 min) with water depth changing from 82 to 130 m. The PF uses a mixed state formulation as explained in Sec. II B with a strongly range-dependent bathymetry and a sediment layer and water column that change slowly compared to the PF steps, mostly following the quickly changing bathymetry.

As mentioned in Sec. II B, the track is split into smaller 10 min intervals with successive PF runs in each section to reduce the maximum size of state dimension. Time between successive filter steps is taken as 1 min. This selection corresponds to a bathymetry point at every ~150 m in range, linearly interpolated in-between, and sediment parameters that follow the bathymetry with a spatial update at each 1.5 km. Similarly, the sound speed EOF coefficients are updated at every 1.5 km. These spatial estimates also are updated continuously as new data become available every minute as

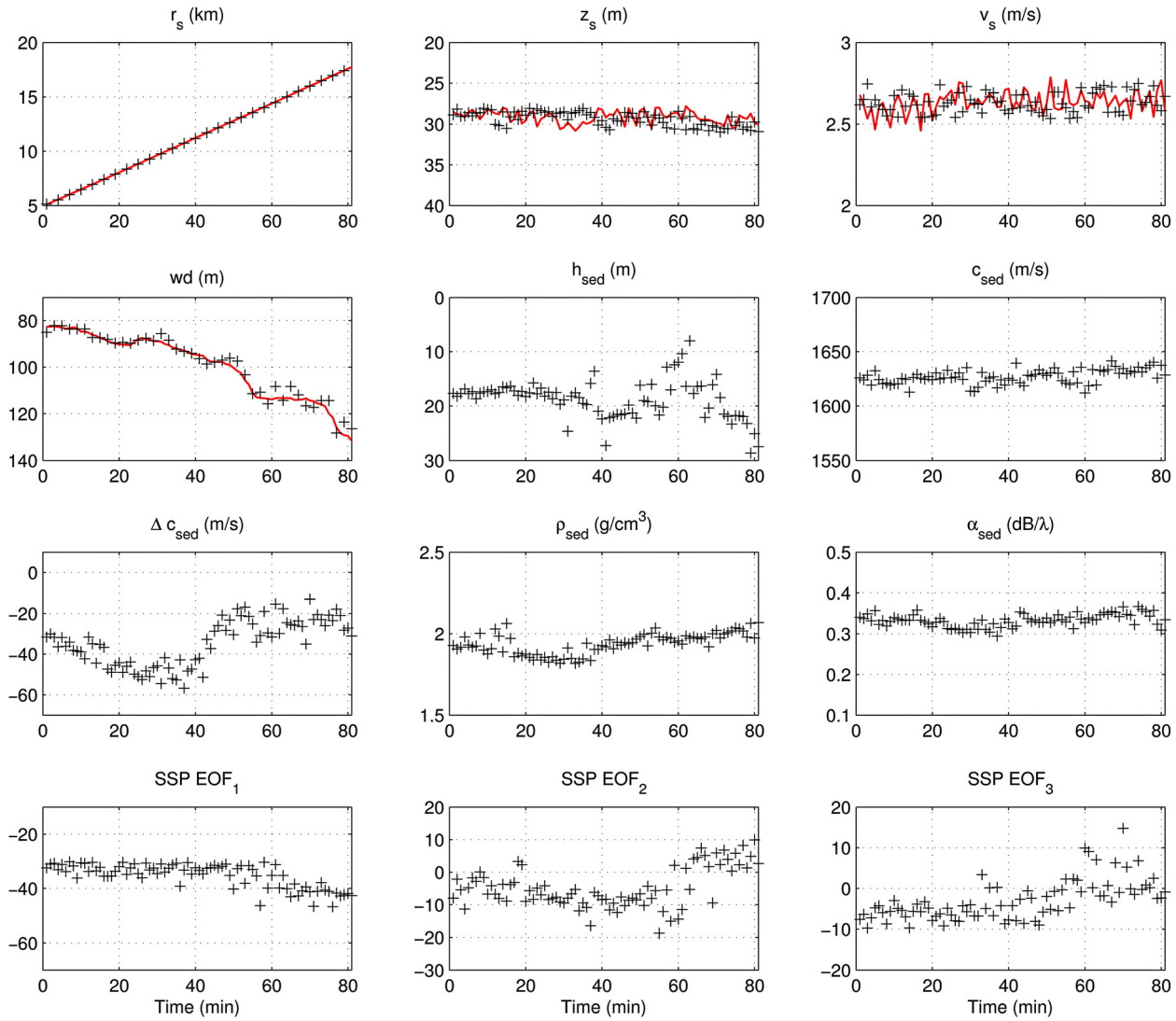

FIG. 6. (Color online) Track II results of source (top) and geoacoustic parameters for PF(+) together with the true trajectories (solid).

shown in Fig. 1. The bottom layer sound speed is assumed constant with a $c_{\text{bot}} = 1740$ m/s and is not tracked.

The ability of PF to handle non-stationary dynamic systems is used here with the state noise variance for the water depth increasing from $\mathbf{Q}_t = (1\,\text{m})^2$ to $(5\,\text{m})^2$ as the source travels toward the shelfbreak. The number of particles is increased gradually from $n_p = 800$ at 5 km to 2000 particles at the end the track.

The environmental model given in Fig. 3 is used at each range. The data are analyzed as in the previous section. The PF is started at a range of 5 km at 02:37 UTC. The data at this location are inverted using a GA and a broad multivariate Gaussian PDF with GA results as the mean is used as the prior to initialize the PF. The inversion at 5 km gave a result similar to Ref. 24 with a decreasing sediment sound speed with depth for the top layer ($\Delta c_{\text{sed}} < 0$). The water column SSP at each range is estimated from estimating the EOF coefficients as with Track I.

The time evolving maximum *a posteriori* (MAP) solution for each parameter is given in Fig. 6. Source parameters are tracked closely. Water depth is well determined too. Sediment thickness stays at 17–18 m for the first 30 min and then fluctuates between 10 and 30 m. The seismic survey images for this shelfbreak[19,20] show that the R-reflector stays mostly less than 25 m below the seafloor. The two-dimensional R-horizon over the region that includes Track I and the first half of Track II can be found in Fig. 1(b) of Ref. 20 as a function of two-way travel time. R-reflector depth values obtained from that plot are in general agreement with the results shown here.

Sound speed at the top of the sediment remains consistent through the track between 1610 and 1645 m/s with an average of 1625 at the beginning of the track gradually moving to 1640 m/s at the end. Unlike the other sediment properties Δc_{sed} shows a distinct range variation. It starts at -30 m/s, corresponding to 1590 m/s at the bottom of the sediment. For 20–40 min the sound speed at the bottom of the sediment layer remains at average 1620 m/s $-$ 50 m/s $=$ 1570 m/s. After 40 min the value evolves to a new average of 1615 m/s, making a vertically more uniform sound speed profile in the sediment. Note that similar shelfbreak results are reported in the literature.[19] The negative gradient in the sediment layer

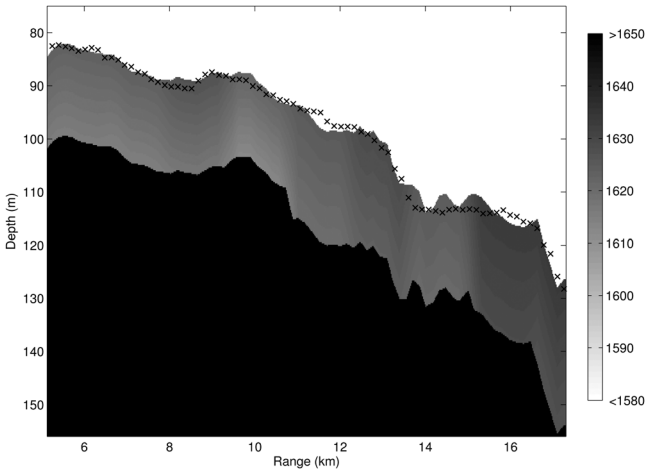

FIG. 7. Track II results. The geoacoustic environment obtained from the MAP estimate sediment sound speed in range and depth. True bathymetry along the ship track given by crosses.

corresponds to the low-speed sediment layer between the erose boundary and the R-reflector.[19]

The range-depth MAP solution for sediment sound speed is shown in Fig. 7, where sound speed for each range and depth along the track is plotted. The PF water depth estimates follow closely the true bathymetry. The marginal distributions for individual parameters are similar to the results for Track I shown in Fig. 5 with a cloud of particles around the MAP values given in Fig. 6.

As discussed earlier, the PF tracks the SSP by tracking the EOF coefficients. In Fig. 8(a), the mean profile used in the EOF analysis, Shark, SW30, and the cloud of particles at 10 min all show similar profiles. The uncertainties in the EOF coefficients at 10 min into the track also are projected into uncertainties in the sound speed as a function of depth as shown in Fig. 8(b).

As the range increases, the estimates fluctuate more, resulting in larger filter divergence probability, likely due to the water column SSP variability. When range increases, the SSP EOF coefficient estimates show greater variability. Although appropriate early in the track, the mean profile and EOFs used are less characteristic of the deeper water SSP later in the track. An extension of this analysis could augment the existing approach with a deeper water mean profile and set of EOFs with coefficients tracked by the PF.

IV. DISCUSSION AND CONCLUSIONS

The capabilities of sequential Bayesian techniques to track source and environmental parameters in spatially and temporally rapidly varying environments such as a shelfbreak region were discussed. Two state models—one for weak range dependence and one for rapid variations—were formulated within the PF. The gradually varying region northwest of the New Jersey shelfbreak was tracked and the results compared favorably with previous Shallow Water 2006 (SW06) inversion results. The SW06 shelfbreak also was tracked over 80–130 m depth.

This paper assumes a single sediment layer and tracks the sound speed in this layer using only one to two parameters. The sediment actually consists of a top sand layer, or has multiple layers.[19,20] It would be possible to use a multiple model PF (Refs. 1 and 8) to track a varying number of layers. However, this would increase the complexity and the state dimension further.

An important issue with geoacoustic inversion at the shelfbreak is the strong variations in the water column SSP.

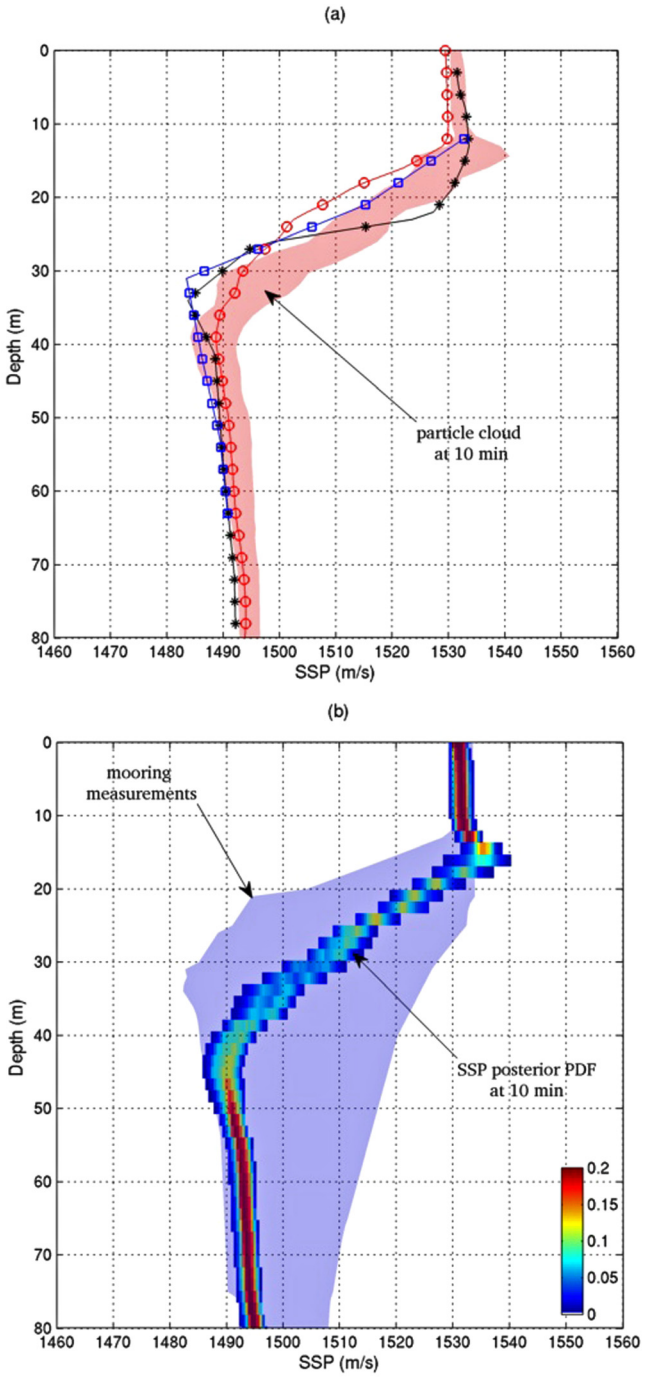

FIG. 8. (Color online) Track II results at 10 min into the track: (a) Particle cloud representing the spread of all particles, along with the mean SSP profile obtained from the CTD analysis (open circles), SSP measurements at Shark (asterisks), and SW30 (open squares) at 10 min (see Fig. 2). (b) Posterior SSP PDF computed by projecting the tracked EOF coefficients represented by the PF particles and weights $\{\mathbf{x}_{10}^i, \mathbf{w}_{10}^i\}_{i=1}^{n_p}$ into sound speed as a function of depth, and the spread of measured SSP profiles from all 11 mooring locations in Fig. 2 during the 80 min track (shown as the mooring measurements).

Large deviations from the underlying model can reduce the geoacoustic inversion/tracking capabilities due to reduced sensitivity of the likelihood function to subbottom parameters. This error can be reduced if the SSP component of the environment model is expanded to accommodate larger spatial variations, however, this will lead to additional computational complexity and increased state dimension.

Strongly range dependent tracks require a large state vector. However, just like other Monte Carlo techniques, PFs are affected by the curse of dimensionality.[35] An alternative would be to employ Kalman filtering, in particular an ensemble Kalman filter (EnKF).[36] The EnKF is a semi-analytic technique designed to handle a large state dimension. The trade-off for employing an EnKF is that all the PDFs must be reduced to Gaussian.

Previous geoacoustic PF studies[6,7] used the SIR PF algorithm without experiencing sample impoverishment.[1,28] Sample impoverishment corresponds to a particle collapse where only one particle has a high likelihood, reducing the posterior PDF to a delta function. Our studies show that impoverishment can be a problem when the strongly range-dependent state formulation is used with a SIR type PF. This is caused by the combination of a large state space and inadequate number of particles. An alternative is to improve sample diversity by using a higher order PF such as a regularized PF (Refs. 1 and 37) or a Markov chain Monte Carlo PF (Ref. 8) at a cost of increased algorithm complexity.

Another issue is filter divergence.[6] Our simulations have shown that divergence is a problem if an insufficient number of particles is used, the true environment evolution is significantly different than the model evolution given by the state equation, the number of environmental parameters is too large, or improper selections are made for state and measurement noise properties.

ACKNOWLEDGMENT

This work was supported by the Office of Naval Research, under Grant Nos. N00014-09-1-0313 and N00014-11-1-0320.

[1]C. Yardim, Z.-H. Michalopoulou, and P. Gerstoft, "An overview of sequential Bayesian filtering in ocean acoustics," IEEE J. Ocean. Eng. **36**, 71–89 (2011).
[2]J. V. Candy and D. H. Chambers, "Model-based dispersive wave processing: A recursive Bayesian solution," J. Acoust. Soc. Am. **105**, 3364–3374 (1999).
[3]E. J. Sullivan, J. D. Holmes, W. M. Carey, and J. F. Lynch, "Broadband passive synthetic aperture: Experimental results," J. Acoust. Soc. Am. **120**, EL49–EL54 (2006).
[4]C. He, J. E. Quijano, and L. M. Zurk, "Enhanced Kalman filter algorithm using the invariance principle," IEEE J. Ocean. Eng. **34**, 575–585 (2009).
[5]O. Carrière, J.-P. Hermand, J.-C. Le Gac, and M. Rixen, "Full-field tomography and Kalman tracking of the range-dependent sound speed field in a coastal water environment," J. Mar. Syst. **78**, S382–S392 (2009).
[6]C. Yardim, P. Gerstoft, and W. S. Hodgkiss, "Tracking of geoacoustic parameters using Kalman and particle filters," J. Acoust. Soc. Am. **125**, 746–760 (2009).
[7]C. Yardim, P. Gerstoft, and W. S. Hodgkiss, "Geoacoustic and source tracking using particle filtering: Experimental results," J. Acoust. Soc. Am. **128**, 75–87 (2010).
[8]J. Dettmer, S. E. Dosso, and C. W. Holland, "Sequential trans-dimensional Monte Carlo for range-dependent geoacoustic inversion," J. Acoust. Soc. Am. **129**, 1794–1806 (2011).
[9]I. Zorych and Z.-H. Michalopoulou, "Particle filtering for dispersion curve tracking in ocean acoustics," J. Acoust. Soc. Am. **124**, EL45–EL50 (2008).
[10]R. Jain and Z.-H. Michalopoulou, "A particle filtering approach for multipath arrival time estimation from acoustic time series," J. Acoust. Soc. Am. **126**, 2249–2249 (2009).
[11]D. Tang, J. N. Moum, J. F. Lynch, P. Abbot, R. Chapman, P. H. Dahl, T. F. Duda, G. Gawarkiewicz, S. M. Glenn, J. A. Goff, H. Graber, J. Kemp, A. Maffei, J. D. Nash, and A. Newhall, "Shallow Water '06: A joint acoustic propagation/nonlinear internal wave physics experiment," Oceanogr. **20**, 156–167 (2007).
[12]Y. Jiang, N. R. Chapman, and M. Badiey, "Quantifying the uncertainty of geoacoustic parameter estimates for the New Jersey Shelf by inverting air gun data," J. Acoust. Soc. Am. **121**, 1879–1894 (2007).
[13]A. Turgut and T. Yamamoto, "In situ measurements of velocity dispersion and attenuation in New Jersey Shelf sediments," J. Acoust. Soc. Am. **124**, EL122–El127 (2008).
[14]J. Yang, D. Tang, and K. L. Williams, "Direct measurement of sediment sound speed in Shallow Water '06," J. Acoust. Soc. Am. **124**, EL116–EL121 (2008).
[15]C. S. Fulthorpe and J. A. Austin, "Shallowly buried, enigmatic seismic stratigraphy on the New Jersey outer shelf: Evidence for latest Pleistocene catastrophic erosion," Geology **32**, 1013–1016 (2004).
[16]J. A. Goff and J. A. Austin, Jr., "Seismic and bathymetric evidence for four different episodes of iceberg scouring on the New Jersey outer shelf: Possible correlation to Heinrich events," Mar. Geol. **266**, 244–254 (2009).
[17]J. Choi, P. Dahl, and J. Goff, "Observations of the R reflector and sediment interface reflection at the Shallow Water '06 Central Site," J. Acoust. Soc. Am. **124**, El128–EL134 (2008).
[18]Y. M. Jiang, N. R. Chapman, and P. Gerstoft, "Short range travel time geoacoustic inversion with a vertical line array," J. Acoust. Soc. Am. **124**, EL135–EL140 (2008).
[19]M. S. Ballard, K. M. Becker, and J. A. Goff, "Geoacoustic inversion for the New Jersey shelf: 3-D sediment model," IEEE J. Ocean. Eng. **35**, 28–42 (2010).
[20]D. P. Knobles, J. A. Goff, R. A. Koch, P. S. Wilson, and J. A. Shooter, "Effect of inhomogeneous sub-bottom layering on broadband acoustic propagation," IEEE J. Ocean. Eng. **35**, 732–743 (2010).
[21]G. R. Potty, J. H. Miller, P. S. Wilson, J. F. Lynch, and A. Newhall, "Geoacoustic inversion using combustive sound source signals," J. Acoust. Soc. Am. **124**, EL146–EL150 (2008).
[22]M. S. Ballard and K. M. Becker, "Geoacoustic inversion on the New Jersey Margin: Along and across the shelf," J. Acoust. Soc. Am. **124**, EL141–EL145 (2008).
[23]D. P. Knobles, P. S. Wilson, J. A. Goff, and S. E. Cho, "Seabed acoustics of a sand ridge on the New Jersey continental shelf," J. Acoust. Soc. Am. **124**, EL151–EL156 (2008).
[24]Y. M. Jiang and N. R. Chapman, "Bayesian geoacoustic inversion in a dynamic shallow water environment," J. Acoust. Soc. Am. **123**, EL155–EL161 (2008).
[25]C.-F. Huang, P. Gerstoft, and W. S. Hodgkiss, "Effect of ocean sound speed uncertainty on matched-field geoacoustic inversion," J. Acoust. Soc. Am. **123**, EL162–EL168 (2008).
[26]F. B. Jensen and M. C. Ferla, "SNAP: The SACLANTCEN normal-mode acoustic propagation model," SACLANT Undersea Research Center, SM–121, La Spezia, Italy (1979), pp. 1–109.
[27]M. D. Collins, "A split-step Padé solution for the parabolic equation method," J. Acoust. Soc. Am. **93**, 1736–1742 (1993).
[28]B. Ristic, S. Arulampalam, and N. Gordon, *Beyond the Kalman Filter: Particle Filters for Tracking Applications* (Artech House, Boston, 2004), Chaps. 1–3.
[29]S. E. Dosso, "Quantifying uncertainty in geoacoustic inversion I. A fast Gibbs sampler approach," J. Acoust. Soc. Am. **111**, 129–142 (2002).
[30]C. F. Mecklenbr̆auker and P. Gerstoft, "Objective functions for ocean acoustic inversion derived by likelihood methods," J. Comput. Acoust. **8**, 259–270 (2000).
[31]C.-F. Huang, P. Gerstoft, and W. S. Hodgkiss, "Uncertainty analysis in matched-field geoacoustic inversions," J. Acoust. Soc. Am. **119**, 197–207 (2006).
[32]C. Yardim, P. Gerstoft, and W. S. Hodgkiss, "Range aliasing in frequency coherent geoacoustic inversion," J. Acoust. Soc. Am. **130**(4), EL154–EL160 (2011).

[33]N. J. Gordon, D. J. Salmond, and A. F. M. Smith, "Novel approach to nonlinear/non-Gaussian Bayesian state estimation," IEE Proc. F, Radar Signal Process. **140**, 107–113 (1993).
[34]J. V. Candy, *Bayesian Signal Processing: Classical, Modern and Particle Filtering Methods* (Wiley, Hoboken, NJ, 2009), Chap. 7.
[35]F. Daum and J. Huang, "Curse of dimensionality and particle filters," in *Proceedings of the IEEE Aerospace Conference* (2003).
[36]O. Carrière, J.-P. Hermand, and J. V. Candy, "Inversion for time-evolving sound-speed field in a shallow ocean by ensemble Kalman filtering," IEEE J. Ocean. Eng. **34**, 586–602 (2009).
[37]C. Musso, N. Oudjane, and F. LeGland, "Improving regularised particle filters," in *Sequential Monte Carlo Methods in Practice*, edited by A. Doucet, N. de Freitas, and N. Gordon (Springer, New York, 2001), Chap. 12.